processes

MDPI

Article

Study on Mechanism of MSWI Fly Ash Solidified by Multiple Solid Waste-Based Cementitious Material Using the Rietveld Method

Xiaoli Wang [1,2], Pingfeng Fu [1,*], Wei Deng [1], JinJin Shi [3] and Miao Xu [4]

[1] School of Civil and Resources Engineering, University of Science and Technology Beijing, Beijing 100083, China; xiaoliwang@ustb.edu.cn (X.W.); dw18821968838@163.com (W.D.)
[2] BGRIMM Technology Group, State Key Laboratory of Mineral Processing, Beijing 102628, China
[3] Cangzhou Municipal Engineering Company Limited, Cangzhou 061000, China; czszjsk@126.com
[4] Road Materials and Technology Engineering Research Center of Hebei Province, Cangzhou 061000, China; czszxm1989@163.com
* Correspondence: pffu@ces.ustb.edu.cn

Abstract: A novel multiple solid waste-based cementitious material (MSWCM) was developed to immobilize municipal solid waste incineration (MSWI) fly ash. The compressive strength of MSWCM with different ratios of MSWI fly ash reached the standard requirements after curing for 28 days. X-ray powder diffraction (XRD) in combination with the Rietveld method was employed to investigate the content and phase transformation of hydration products. The main hydration products of pure MSWCM paste were C-S-H, hydroxyapatite, ettringite and C-A-S-H. With increases in curing time, the content of ettringite and C-A-S-H increased significantly. The main hydration products of MSWCM paste with MSWI fly ash were C-S-H and Friedel's salt. The contents increased markedly with increased curing time from 21.8% to 28.0% and from 8.53% to 16.7%, respectively. Additionally, a small amount of $PbHPO_4$ (0.51–0.96%) and lead phosphate $Pb_3(PO_4)_2$ (0.14–0.51%) were detected, indicating that phosphate had an effective curing effect on lead ions. The results showed that most of the hydration reactions had started at the initial stage of curing and reacted quickly to form a large number of hydration products. The quantitative analyses of hydration products provide essential information for understanding the immobilization mechanism of MSWI fly ash in MSWCM paste.

Keywords: cementitious material; MSWI fly ash; Rietveld method; multiple solid waste; heavy metals; solidification; X-ray diffraction

Citation: Wang, X.; Fu, P.; Deng, W.; Shi, J.; Xu, M. Study on Mechanism of MSWI Fly Ash Solidified by Multiple Solid Waste-Based Cementitious Material Using the Rietveld Method. *Processes* **2023**, *11*, 2311. https://doi.org/10.3390/pr11082311

Academic Editor: Hsin Chu

Received: 28 June 2023
Revised: 22 July 2023
Accepted: 26 July 2023
Published: 1 August 2023

1. Introduction

Urbanization, population growth and industrialization have led to a rapid increase in municipal solid waste. By 2025, cities worldwide are expected to generate 2.2 billion tons of municipal solid waste [1]. Landfill and incineration are the two main waste disposal methods. Compared with landfill, the incineration method can save land resources. After incineration, the volume of municipal waste can be significantly reduced, and the heat generated by the complete incineration of organic matter can be used for heating and power generation, realizing the resource utilization of waste [2–5]. Therefore, the incineration method has been commonly used in the treatment of municipal waste. However, it tends to produce a large amount of municipal solid waste incineration (MSWI) fly ash. The level of MSWI has reached 146 million tons in China in 2020 and the production of MSWI fly ash has exceeded 7 million tons [6]. MSWI fly ash is produced during waste incineration. It contains a large amount of hazardous substances, such as leachable heavy metals, dioxins, soluble salts and other harmful components, which may cause harm to the environment and human health [7–10]. It can used in landfill only after solidification or stabilization [11–13].

Cement-based stabilization or solidification technology has been considered as the main treatment option for MSWI fly ash [14–17]. Ordinary Portland Cement (OPC) is

a widely used cementitious binder for the treatment of MSWI fly ash [18,19]. However, OPC will form a strong alkaline environment that is not conducive to the solidification of heavy metals. The compressive strength of OPC–fly ash blocks may decrease significantly in the case of high waste incineration fly ash content. [20–22]. In addition, during the production process of Portland cement, some problems will become more prominent, such as pollutant discharge, excessive consumption of energy resources and damage to the balance of the ecological environment [23,24]. Therefore, it is necessary to develop a low carbon environment-friendly binder material.

Recently, due to excellent mechanical properties and good environmental protection, the cementitious material produced from multiple solid wastes, such as metallurgical slags and industrial solid wastes, has been widely used to treat various hazardous wastes including MSWI fly ash [25,26]. Blast furnace slag (BFS) and steel slag (SS) are commonly used metallurgical slags for solid waste-based cementitious material, and the main components are CaO, SiO_2 and Al_2O_3 [27]. BFS and SS can be used as an alternative material for alkaline activator because they are alkaline, which can provide Ca^{2+} ions and OH^- ions for the hydration reaction [28]. Desulfurization ash (DA) is a solid waste generated during the dry flue gas desulfurization process, with CaO and SO_3 as the main components [29,30]. Phosphoric acid sludge (PAS) is an industrial solid waste obtained from the production of wet phosphoric acid [31,32]. PAS can be used to immobilize MSWI fly ash due to the widespread use of phosphate as a curing agent [33–35]. Additionally, Pb can easily react with PO_4^{3-} and HPO_4^{2-} to form insoluble phosphate precipitation [33]. Therefore, phosphate shows a good solidification effect on Pb. These industrial solid wastes can be used as the raw materials of multiple solid waste-based cementitious material (MSWCM).

During the hydration process, heavy metals react with MSWCM through physical cementation, chemical adsorption, isomorphic replacement and complex precipitation. Finally, they settle in the cement hydration product in the form of hydroxide or complex [33]. The quantitative and qualitative analyses of mineral phases provide essential information for understanding the immobilization mechanism of MSWI fly ash in MSWCM paste. However, the study of assessing the mineral composition of fly ash and hydration products by conventional X-ray powder diffraction (XRD) has been hampered due to the complex phases and structures, which result in strong overlap of diffraction peaks [36]. Therefore, it is necessary to find a method that can determine the relative content of the mixture phase and hydration products accurately, effectively and conveniently in MSWCM.

XRD in combination with the Rietveld refinement method, is a powerful technique for the characterization of mineral phases. The Rietveld method is basically a profile-fitting method based on the least square approach, which can deal with complex diffraction patterns with strong overlapping peaks [37]. However, few studies have focused on using the Rietveld methods to study changes in the content of hydration products and mineral phases during hydration process.

In this study, blast furnace slag (BFS), steel slag (SS), desulfurization ash (DA) and phosphoric acid sludge (PAS) are used as raw materials to produce a novel multiple solid waste-based cementitious material (MSWCM). The development of the mechanical properties of MSWCM with different ratios of MSWI fly ash, including compressive strength and leachability at different curing times, is investigated. The Rietveld method is employed for the qualitative and quantitative analysis of the MSWI fly ash and of the hydration products in pure MSWCM pastes and pastes containing MSWI fly ash. Meanwhile, the changes in the hydration products and mineral phase content during the hydration process and the immobilization mechanism of MSWI fly ash in MSWCM pastes are also discussed.

2. Materials and Methods

2.1. Materials

Raw materials for the preparation of multiple solid waste-based cementitious material (MSWCM) included blast furnace slag (BFS), steel slag (SS), desulfurization ash (DA) and phosphoric acid sludge (PAS). The BFS, SS and DA were provided by Wuhan Metal

Resources Company in Hubei Province, China. The PAS was collected from China City Environment Protection Engineering Limited Company. The chemical compositions and heavy metal content of the four raw materials were summarized in a previous study [27]. CaO, SiO_2 and Al_2O_3 were the major chemical compositions. Furthermore, the desulfurization ash contained 33.28% SO_3, the steel slag contained 26.12% Fe_2O_3 and the phosphoric acid sludge contained 21.80% P_2O_5. It had a high content of Pb (2412.81 mg/kg), which was the main heavy metal.

2.2. Orthogonal Experiment and Analysis

2.2.1. Orthogonal Experimental Design

Orthogonal experimental design is a method to study multi-factor and multi-level experiments. An orthogonal experiment was designed to optimize the mass ratio of the raw materials for the production of the MSWCM. The mass proportions of SS, DA and PAS were set as the three factors in the orthogonal experiment. The level settings of each factor are shown in Table 1. The mass proportion of BFS was calculated by [100% − (SS% + DA% + PAS%)]. The standard orthogonal experimental design table L16 (43) was used and a total of 16 themes were tested. The orthogonal experimental design is displayed in Table 2.

Table 1. Factors and levels for orthogonal test.

Levels	Factors		
	Mass Proportions		
	SS/%	DA/%	PAS/%
1	28	8	20
2	32	10	26
3	36	12	32
4	40	14	38

Table 2. Experimental design schemes of orthogonal test.

Sample ID	Levels			Mass Proportion of BFS/%
	SS	DA	PAS	
O1	1	1	1	44
O2	1	2	2	36
O3	1	3	3	28
O4	1	4	4	20
O5	2	1	2	34
O6	2	2	1	38
O7	2	3	4	18
O8	2	4	3	22
O9	3	1	3	24
O10	3	2	4	16
O11	3	3	1	32
O12	3	4	2	24
O13	4	1	4	14
O14	4	2	3	18
O15	4	3	2	22
O16	4	4	1	26

2.2.2. Range Analysis Method

In this study, the range analysis method was used to determine the factors' sensitivity to compressive strength according to the orthogonal experiment [38]. The range method is to subtract the minimum value from the maximum value in the data. In the calculation, the average value k_i and the influence degree R are as follows [39]:

$$k_i = \frac{K_i}{x} \quad (1)$$

$$R = max\{k_1, k_2, k_3 \cdots\} - min\{k_1, k_2, k_3 \cdots\} \quad (2)$$

where, k_i is the arithmetic mean value of the corresponding test results at level i; K_i is the sum of the corresponding test results; and x is the number of tests on level i. The influence degree R represents the influence of each factor on the index. The higher the R value, the greater the influence of the factor on the experiment results.

2.3. Compressive Strength Test

Compressive strength was measured in an electro-hydraulic universal testing machine (WAW-1000B) in compliance with the GB/T17671 [27] China standard. The measurements were performed on specimens for 3, 7 and 28 days at room temperature and at least three representative samples were tested to obtain the average values.

2.4. Leaching Test

The leaching toxicity of the heavy metals was evaluated by the Solid Waste-Extraction Procedure for Leaching Toxicity—Horizontal Vibration Method (HJ 557-2010). The samples were first crushed to below 3 mm, then 100 g was taken and put into a 2 L volumetric flask, and we added 1000 mL of deionized water. After that, the mixtures were put into a horizontal vibrator for 8 h with a frequency of 110 times per minute. After standing still for 16 h, the concentrations of heavy metals in the leachate were determined by inductively coupled plasma mass spectrometry (ICP-MS).

2.5. X-ray Powder Diffraction (XRD) Analysis

The phase analysis of the samples was determined by the X-ray powder diffraction (XRD) method. The XRD patterns were collected by an Rigaku D/Max-B diffractometer with an X'Celerator detector and using Cu Kα radiation (λ = 0.154056 nm), 40 kV and 40 mA. The measured range of the powder specimens was set from 5 to 80° 2θ, with a 0.04° step size.

2.6. Rietveld Method

The Rietveld method is an advantageous technique for the refinement of crystal structures and phase quantitative analysis. This method was employed to determine the major phases of the MSWI fly ash and the hydration products during solidification in this study. The principle of the Rietveld method is to minimize the difference between the observed and calculated intensities by a least square approach (Equation (3)). The BGMN program was used for the Rietveld refinement [40,41]:

$$\sum_i w_i [y_i(obs) - y_i(calc)]^2 = \text{Minimum} \quad (3)$$

where yi (obs) and yi ($calc$) are the observed and calculated intensities at point i, and w_i is the weight assigned to each intensity. The intensity at each point is calculated by summing the contributions from all the neighboring Bragg reflections and background scattering:

$$y_i = S \sum_k \left[|F_{hkl}|^2 \cdot G(\Delta 2\theta) \cdot Lp(\theta) \cdot M_{hkl} \cdot T_f(\theta) \cdot A \cdot Po_{hkl} \right] + y_{bi} \quad (4)$$

where y_i intensity of the angular position i in the powder pattern;

S—scale factor of the phase;
F_{hkl}—structure factor;
G($\Delta 2\theta$)—profile shape function;
$Lp(\theta)$—Lorentz and Polarization factor;
M_{hkl}—multiplicity factor;
$T_f(\theta)$—temperature factor;
A—absorption factor;
Po_{hkl}—correction factor of preferred orientation;

y_{bi}—background intensity.

3. Results and Discussion

3.1. Characterization of MSWI Fly Ash

Municipal solid waste incineration (MSWI) fly ash was collected from MSWI plants in Wuhan, China. The main chemical composition and heavy metal contents are given in Table 3. According to the results, CaO accounted for the largest proportion of MSWI fly ash, accounting for 39.08%, followed by Cl (21.5%) and Na_2O (7.03%). This is probably due to the addition of alkali to neutralize the acidic gases generated during incineration, such as HCl and SO_2 [42]. The high content of chloride ion may be attributed to the incineration of plastics and halite in food residues, e.g., NaCl [43,44]. The most abundant heavy metals are Pb and Zn, with a content of 1769.9 mg/kg and 5636.2 mg/kg, respectively.

Table 3. Chemical composition and heavy metal content of MSWI fly ash.

Oxide (%)	**CaO**	**SiO_2**	**Al_2O_3**	**Cl**	**SO_3**	**Fe_2O_3**	**Na_2O**	**K_2O**	**MgO**
	39.08	1.94	0.31	29.17	7.37	1.46	7.03	10.58	0.56
Heavy metal (mg/kg)	**Pb**	**Zn**	**As**	**Cr**	**Hg**				
	1769.9	5636.2	45.7	34.3	2.4				

The phase content of the MSWI fly ash was determined by the Rietveld method. Figure 1 presents the Rietveld refinement plot for the MSWI fly ash. The measured patterns showed good agreement with the calculated patterns. The R_{wp} value was 10.25%. According to the results, the main phases in the MSWI fly ash were NaCl (34.2%), CaClOH (24.6%), $Ca(OH)_2$ (16.5%) and KCl (14.3%) (Table 4). Moreover, $CaCO_3$ and $CaSO_4$ were also detected.

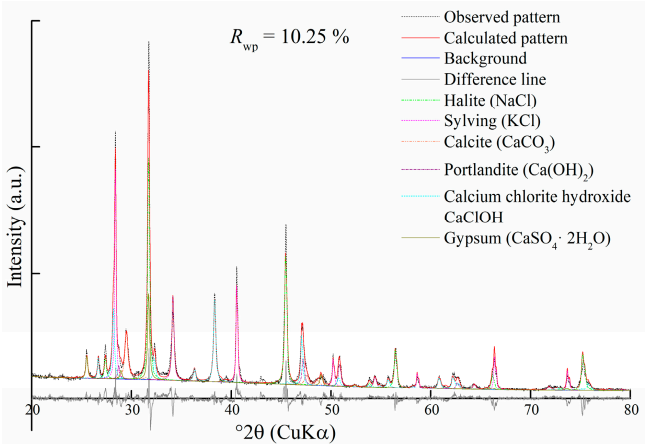

Figure 1. Rietveld refinement plot for MSWI fly ash.

Table 4. Results of the Rietveld refinement of MSWI fly ash.

	Halite	**Sylving**	**Calcium Chloride Hydroxide**	**Portlandite**	**Calcite**	**Gypsum**	**R_{wp}/%**	**R_{exp}/%**
	NaCl	**KCl**	**CaClOH**	**$Ca(OH)_2$**	**$CaCO_3$**	**$CaSO_4 \cdot 2H_2O$**		
Phase content/w.t.%	34.2 (2) [a]	14.3 (1)	24.6 (2)	16.5 (1)	7.6 (5)	2.8 (7)	10.25	5.26

[a] Standard deviation.

3.2. Orthogonal Experiment Results Analysis

The range analysis method was adopted for the orthogonal experiment results. The *R* value (Range) is used to divide the impact degree of different factors on the experimental objectives. Figure 2 and Table 5 present the results of the orthogonal experiment and range analysis. According to the *K* value, the optimal combination of factors and levels is SS_2 DA_3 PAS_1, and their corresponding mass proportions are 32%, 12% and 20%, respectively. The mass proportion of BFS is calculated as 36%. As shown in Table 5, the order of the *R* value is PAS > SS > DA, indicating that the mass ratio of PAS is the dominant factor affecting the compressive strength, followed by the mass ratios of SS and DA.

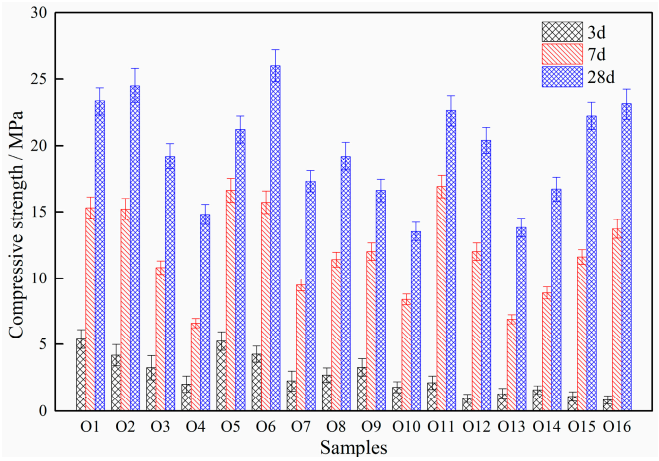

Figure 2. The result of orthogonal experiment.

Table 5. The result of range analysis.

Levels	Compressive Strength/Mpa		
	SS	**DA**	**PAS**
K1	81.8	74.9	95
K2	83.7	80.7	81.4
K3	73.1	81.3	71.7
K4	75.8	77.5	66.3
k1	20.45	18.73	23.75
k2	20.93	20.18	20.35
k3	18.28	20.33	17.93
k4	18.95	19.38	16.58
Range	2.65	1.6	7.17
Ranking		PAS > SS > DA	
Optimum theme		SS_2 DA_3 PAS_1	

Figure 3 shows the effect curves of different raw materials on the compressive strength. Based on the results, the influence of the PAS ratio on the compressive strength is the greatest. The compressive strength decreases with increases in the PAS mass ratio. However, the compressive strength shows a tendency to first increase and then decrease with increases in the DA mass ratio. The effect of the SS mass ratio on the compressive strength is fluctuating.

3.3. Effect of MSWI Fly Ash Proportions on Compressive Strength

The compressive strength of multiple solid waste-based cementitious material (MSWCM) with different amounts of MSWI fly ash is plotted in Figure 3. The compressive strength increased with curing time for all specimens and, after curing for 3, 7 and 28 days, the compressive strength varied from 1.2 to 33.4 MPa, which all met the standard requirements of Chinese technical standards for the solidification/stabilization treatment of MSWI fly ash. The compressive strength of the MSWCM pastes without MSWI fly ash had reached

27.2, 28.6 and 33.4 MPa after curing for 3, 7 and 28 days, respectively. It was noticed that the 7-day compressive strength was 81.4% of the 28-day strength, indicating a rapid early strength development.

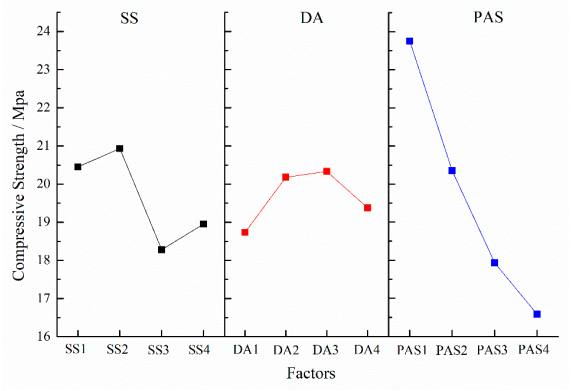

Figure 3. Effect of different raw materials on compressive strength.

According to Figure 4, the compressive strength showed a tendency to decrease with increases in MSWI fly ash content. In comparison with the MSWCM pastes after a 28-day curing period, the compressive strength of the MSWCM pastes decreased by 4.2%, 17.3%, 27.5%, 45.5%, 57.5%, 72.2%, 82.6% and 91.3%, respectively, with an increase in MSWI fly ash content from 10% to 80%. The addition of MSWI fly ash had a negative impact on the compressive strength of the MSWCM pastes, mainly due to the lower activity of MSWI fly ash and the high level of heavy metals, which inhibited the hydration reaction and weakened the compressive strength [42,45,46].

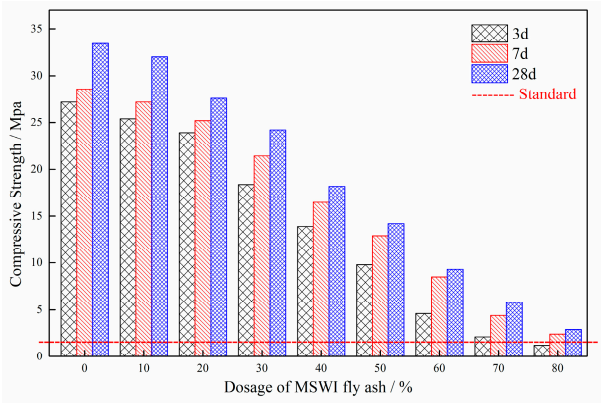

Figure 4. Compressive strength of MSWCM pastes with MSWI fly ash.

3.4. Leaching Toxicity

The leaching concentrations of As, Cr, Pb and Zn of the MSWCM pastes with MSWI fly ash at 3, 7 and 28 curing days are given in Figure 5. With increases in MSWI fly ash content, the leaching concentration of As, Cr and Pb increased. The pure MSWCM pastes showed a low leaching concentration of these four heavy metals. The maximum leaching concentrations of As, Cr, Pb and Zn were 22.6 μg/L, 12.5 μg/L,113.0 μg/L and 75.6 μg/L, respectively, which were far below the Toxicity Characteristic Leaching Procedure (TCLP) standard requirement and the threshold value specified in Standard GB16889-2008. This indicated that MSWCM can effectively immobilize these heavy metals.

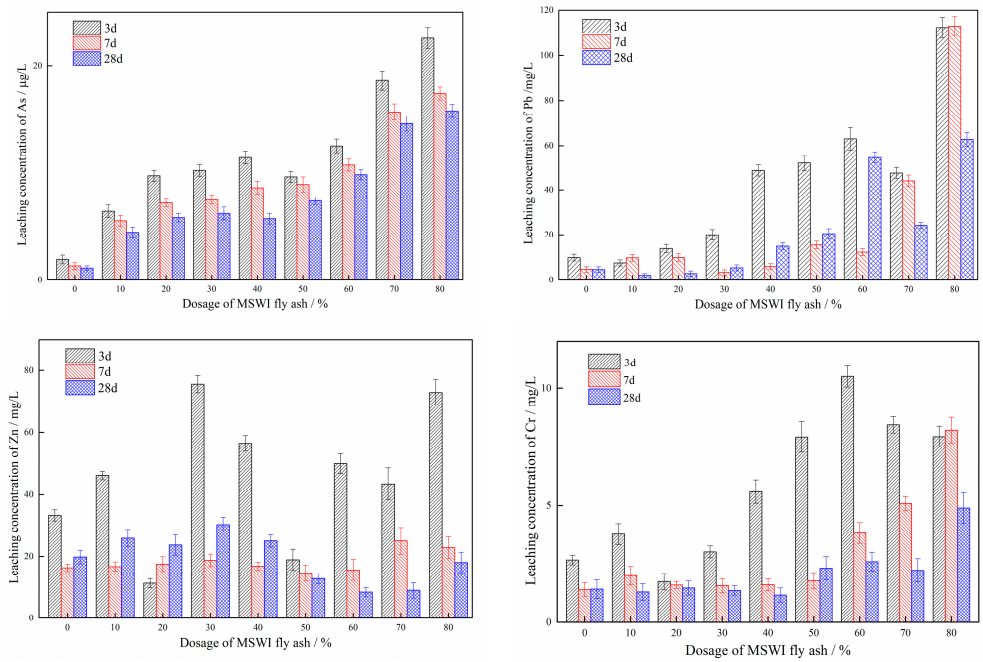

Figure 5. Leaching concentrations of heavy metals in MSWCM solidified body with different MSWI fly ash content.

MSWCM after curing with MSWI fly ash can be used as a supplementary cementitious material, replacing or partially replacing traditional cement and other cementitious materials. This type of cementitious material can be widely used in various applications, such as roadbed materials, landfill closure and ground hardening.

3.5. Characterization of MSWCM Hydration Products with and without MSWI Fly Ash

3.5.1. XRD Analysis of Hydration Products

The XRD patterns of the pure MSWCM pastes (MF0) and the MSWCM pastes with 30% MSWI fly ash (MF1) at a curing time of 3, 7 and 28 days are shown in Figure 6 and the main mineral phases have been labelled. According to the diffraction pattern, the diffraction peak with the strongest intensity in the pure MSWCM pastes belonged to calcium carbonate, and the main hydration products were hydroxyapatite, ettringite and calcium silicate hydrate (C-S-H and C-A-S-H).

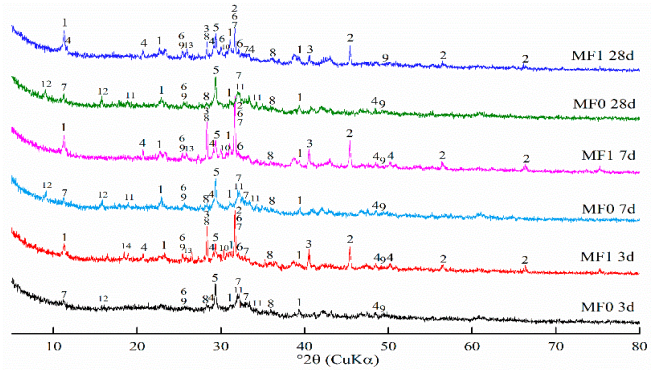

Figure 6. XRD patterns of MF0 and MF1 samples with different curing times. The main peaks are labelled as follows: 1-Friedel's salt ($3CaO{\cdot}Al_2O_3{\cdot}CaCl_2{\cdot}10H_2O$); 2-Halite (NaCl); 3-Sylvite (KCl); 4-Gypsum ($CaSO_4{\cdot}2H_2O$); 5-Calcite ($CaCO_3$); 6-C-S-H; 7-Hydroxyapatite ($Ca_5(PO_4)_3(OH)$); 8-C-A-S-H; 9-PbO_2; 10-$PbHPO_4$; 11-C_2S ($2CaO{\cdot}SiO_2$); 12-Ettringite ($3CaO{\cdot}Al_2O_3{\cdot}3CaSO_4{\cdot}32H_2O$); 13-$Pb_3(PO_4)_2$; 14-Carnallite ($KCl{\cdot}MgCl_2{\cdot}6H_2O$).

In contrast, strong peaks for chlorine salts such as halite and sylvite were observed in the samples mixed with 70% MSWCM and 30% MSWI fly ash. Additionally, some new hydrates such as Friedel's salt ($3CaO{\cdot}Al_2O_3{\cdot}CaCl_2{\cdot}10H_2O$), $PbHPO_4$ and $Pb_3(PO_4)_2$ were formed. The diffraction peaks intensity of the Friedel's salt increased significantly with increases in curing time. Meanwhile, the diffraction peaks of the halite (NaCl) and sylvite (KCl) gradually weakened with the increase of Friedel's salt. It can be deduced that chloride salts might be partially transformed into Friedel's salt, which indicated that part of the Cl in MSWI fly ash could be encapsulated in the MSWCM solidified body. The generation of $PbHPO_4$ and $Pb_3(PO_4)_2$ in sample MF1 indicated that the Pb took part in a chemical reaction with phosphate and then formed insoluble lead phosphate minerals. This conclusion was consistent with [42] and confirmed that phosphate shows a good solidification effect on Pb.

Furthermore, calcium-containing hydration products (C-S-H and C-A-S-H) were found in both the MF0 and MF1 samples, and the intensity of these diffraction peaks in sample MF1 is significantly stronger than that in sample MF0. However, no distinct peaks of portlandite were observed in the MF0 and MF1 samples. It is indicated that these hydration products were further hydrated with the components in the MSWI fly ash.

3.5.2. Immobilization Mechanism Analysis using Rietveld Method

Although the main mineral composition can be obtained by traditional XRD analysis, it is difficult to identify minor minerals and their content, and the accuracy of the results is not high. The qualitative and quantitative phases of the MSWCM pastes with MSWI fly ash are crucial for understanding the hydration process and the hydration mechanism. Therefore, the Rietveld method was employed in this work to investigate the mineral composition and content and the mineral phase transformation of the hydration products.

The mineralogical compositions and quantitative analysis of the hydration products in the MSWCM pastes (MF0) without or with MSWI fly ash (samples MF0 and MF1) at a curing time of 3, 7 and 28 days are presented in Tables 6 and 7. The quality of the Rietveld fitting was evaluated by the weighted profile factor R_{wp} and the expected factor R_{exp}. Figure 7 shows the refinement results of samples MF0 and MF1 after curing for 28 days. The calculated patterns of these two samples showed comparatively good agreement with the measured patterns. The refinements of samples MF0 and MF1 after curing different days achieved R_{wp} values in the range of 7.35% to 7.55% and 7.70% to 7.81%, and R_{exp} values in the range of 5.85% to 5.90% and 6.01% to 6.12%, respectively. It is indicated that the refinement results for these samples were acceptable and reasonable.

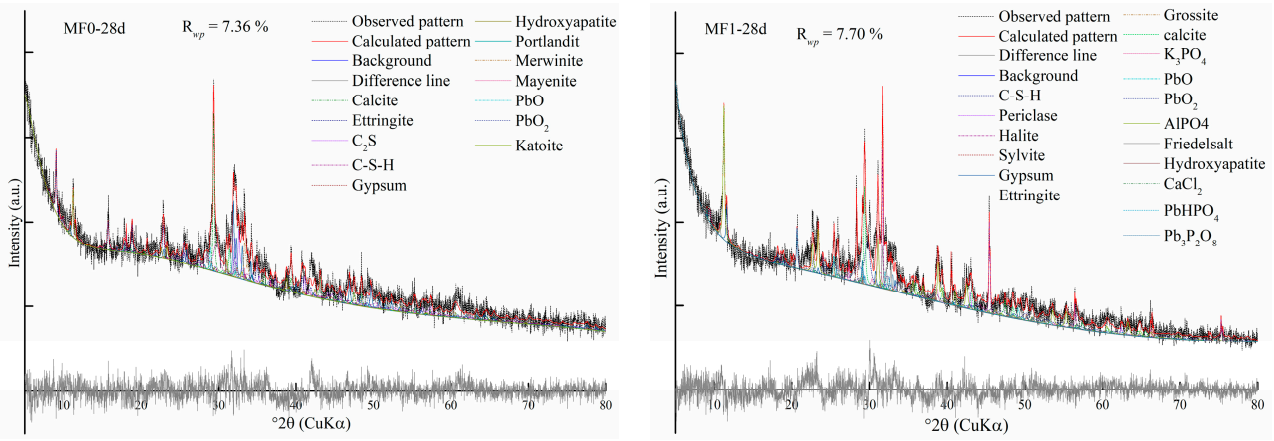

Figure 7. Rietveld refinement of samples MF0 and MF1 after curing for 28 days.

Pure MSWCM Paste

As shown in Table 6, the pure MSWCM paste without MSWI fly ash (sample MF0) contained C_2S (17.85–20.55%) and calcite (12.59–14.71%). The main hydration products

of sample MF0 were C-S-H ($Ca_5Si_6O_{16}(OH)\cdot 4H_2O$), hydroxyapatite ($Ca_5(PO_4)_3(OH)$) and ettringite ($3CaO\cdot Al_2O_3\cdot 3CaSO_4\cdot 32H_2O$).

The hydration reaction of C_2S and C_3S in the raw material produced calcium silicate hydrate (C-S-H) and calcium hydroxide (Equations (5) and (6)). The hydration reaction of C_2S is much slower than that of C_3S. Therefore, after 28 days of curing, there was still unreacted C_2S. The content of C-S-H and hydroxyapatite at different curing times was in the range of 19.8–24.7% and 11.29–19.87%, respectively. It can be seen from the results that a large amount of C-S-H and hydroxyapatite have been formed when the curing time is 3 days. This is very beneficial to the improvement of compressive strength and the solidification of MSWI fly ash. The generated alkaline activator $Ca(OH)_2$ can destroy and dissolve the silica vitreous structure and increase the amount of Ca^{2+}, Al^{3+} and $SiO_4{}^{2-}$. This may accelerate the hydration reaction, resulting in higher early compressive strength. With the continuous accumulation of various ions in the liquid phase, the solution reaches the supersaturated state of new hydration products, thus generating new hydration products. For example, $Ca(OH)_2$ further reacts with Al_2O_3 and $CaSO_4$ to form ettringite and a small amount of C-A-S-H ($3CaO\cdot Al_2O_3\cdot 2SiO_2\cdot 2H_2O$) (Equations (7) and (8)). The generated C-A-S-H content was 2.35–4.71%. Compared with the C-A-S-H, the content of generated ettringite was relatively large, and with the prolonging of the curing time the content increased significantly. Its content were 4.15%, 17.9% and 16.9% at a curing time of 3, 7 and 28 days, respectively. It indicated that the hydration process was constantly evolving.

In addition, $PO_4{}^{3-}$ produced from phosphoric acid sludge (PAS) reacted with Ca^{2+} in the aqueous solution to form a new hydration product, hydroxyapatite ($Ca_5(PO_4)_3(OH)$) (Equation (9)). The content of hydroxyapatite was 19.87%, 13.40% and 11.29% at a curing time of 3, 7 and 28 days, respectively. The possible hydration reactions that occurred in the pure MSWCM paste samples were listed as follows:

$$2C_3S + 6H_2O \rightarrow 3C-S-H + 3Ca(OH)_2 \quad (5)$$

$$2C_2S + 4H_2O \rightarrow 3C-S-H + Ca(OH)_2 \quad (6)$$

$$3Ca(OH)_2 + Al_2O_3 + 3CaSO_4\cdot H_2O + 23H_2O \rightarrow 3CaO\cdot Al_2O_3\cdot 3CaSO_4\cdot 32H_2O \quad (7)$$

$$Ca(OH)_2 + Al_2O_3 + SiO_2 + H_2O \rightarrow CaO\cdot SiO_2\cdot Al_2O_3\cdot (n+1)H_2O\ (C-A-S-H) \quad (8)$$

$$5Ca^{2+} + 4OH^- + 3HPO_4^{2-} \rightarrow Ca_5(PO_4)_3(OH) + H_2O \quad (9)$$

Some heavy metal oxides were detected at very low levels, such as PbO (0.17–0.3%) and PbO_2 (0.43–0.52%). And, after curing for 28 days, a small amount of mayenite ($12CaO\cdot 7Al_2O_3$) (0.55%) appeared.

The mineral phase quantitative analysis of MSWCM paste with MSWI fly ash (sample MF1) under different curing times using the Rietveld method is listed in Table 7. It can be seen from the results that the phase composition is relatively complex. The dominant mineral phases were C-S-H, halite, sylvite, Friedel's salt, K_3PO_4, hydroxyapatite, $AlPO_4$, calcite and gypsum, while the minor mineral phases were portlandite, periclase, mayenite, ettringite, grossite, katoite, PbO_2, $CaCl_2$, $PbHPO_4$ and lead phosphate (Table 7).

The main hydration products of sample MF1 were C-S-H ($Ca_5Si_6O_{16}(OH)\cdot 4H_2O$) and Friedel's salt ($3CaO\cdot Al_2O_3\cdot CaCl_2\cdot 10H_2O$). The content of C-S-H and Friedel's salt increased significantly with increases in curing time and their contents were 21.8%, 26.2% and 28.0% and 8.53%, 12.68% and 16.17% after the curing time of 3, 7 and 28 days, respectively. This result is consistent with the intensity variation of the diffraction peaks (Figure 6). At the same time, the amount of halite (NaCl) and sylvite (KCl) is decreasing, further illustrating the effect of Friedel's salt on the solidification of the chloride ions in the MSWI fly ash. C-S-H

has been proved to immobilize heavy metals (such as Zn, Cd and Pb) effectively [33]. With increases in curing time, the content of C-S-H increased, the stabilization efficiency should be better. This is consistent with the leaching results shown above (Figure 5). Additionally, the more C-S-H generated, the more beneficial it is to improve the compressive strength. This is consistent with the growth trend in Figure 3. In addition, there was a small amount of C-A-S-H ($3CaO{\cdot}Al_2O_3{\cdot}2SiO_2{\cdot}2H_2O$) generated, the content of which is 2.54–4.22% at different curing times.

Table 6. Quantitative results of sample MF0 using the Rietveld method.

Minerals	Chemical Formula	Rietveld Quantitative Results Contents/Mass %		
		3 d R_{wp} = 7.55% R_{exp} = 5.88%	**7 d** R_{wp} = 7.35% R_{exp} = 5.85%	**28 d** R_{wp} = 7.36% R_{exp} = 5.90%
Calcite	$CaCO_3$	14.70 (1) [a]	13.78 (1)	12.59 (1)
Ettringite	$3CaO{\cdot}Al_2O_3{\cdot}3CaSO_4{\cdot}32H_2O$	4.15 (1)	17.90 (1)	16.90 (1)
C_2S	$2CaO{\cdot}SiO_2$	20.10 (1)	20.55 (1)	17.85 (1)
C-S-H	$Ca_5Si_6O_{16}(OH){\cdot}4H_2O$	24.70 (2)	17.80 (2)	19.80 (2)
Gypsum	$CaSO_4{\cdot}2H_2O$	4.08 (1)	3.09 (1)	4.23 (1)
Hydroxyapatite	$Ca_5(PO_4)_3(OH)$	19.87 (1)	13.40 (1)	11.29 (1)
Portlandite	$Ca(OH)_2$	0	0	0
Merwinite	12CaO·7Al2O3	9.79 (1)	9.37 (1)	11.44 (1)
Mayenite	$Ca_{12}Al_{14}O_{33}$	0	0.39 (2)	0.55 (2)
PbO	-	0.30 (1)	0.16 (1)	0.21 (1)
PbO_2	-	0	0.48 (1)	0.47 (1)
C-A-S-H	$3CaO{\cdot}Al_2O_3{\cdot}2SiO_2{\cdot}2H_2O$	2.35 (1)	3.07 (1)	4.71 (1)
sum		100.04	100.00	100.04

[a] Standard deviation.

MSWCM Paste with MSWI Fly Ash

Halite (NaCl) and sylvite (KCl) were the main phases in the MSWI fly ash (Figure 1). NaCl can react with calcium aluminate hydrate to form Friedel's salt ($3CaO{\cdot}Al_2O_3{\cdot}CaCl_2{\cdot}10H_2O$) (Equation (10)) and potassium ions may form potassium phosphate (K_3PO_4) (Equation (11)). The content of halite and sylvite decreased with increases in curing days (Table 7). This suggested that some chloride ions in MSWI fly ash could be encapsulated in MSWCM paste by a chemical bonding effect.

A small amount of $PbHPO_4$ (0.51–0.96%) and lead phosphate $Pb_3(PO_4)_2$ (0.14–0.51%) were detected. Irene et al. and Ren et al. [35,47] found that the presence of phosphate was beneficial for the formation of insoluble lead phosphate salts (Equations (12) and (13)). Compared with other heavy metal ions, such as Zn, Cr and As, the phosphate ions reacted preferentially with Pb [48]. Due to the very low solubility of lead phosphate salts, Pb can be stably solidified in MSWCM paste and have a good curing effect. The quantitative change of the main hydration products is shown in Figure 8.

$$Al_2O_3 + 4CaO + 2NaCl + 11H_2O \rightarrow 3CaO{\cdot}Al_2O_3{\cdot}CaCl_2{\cdot}10H_2O + NaOH \quad (10)$$

$$PO4^{3-} + 3OH^- + 3K^+ \rightarrow K_3(PO_4) + 3H_2O \quad (11)$$

$$2PO4^{3-} + 3Pb^{2+} \rightarrow Pb_3(PO_4)_2 \quad (12)$$

$$HPO4^{2-} + Pb^{2+} \rightarrow PbHPO_4 \quad (13)$$

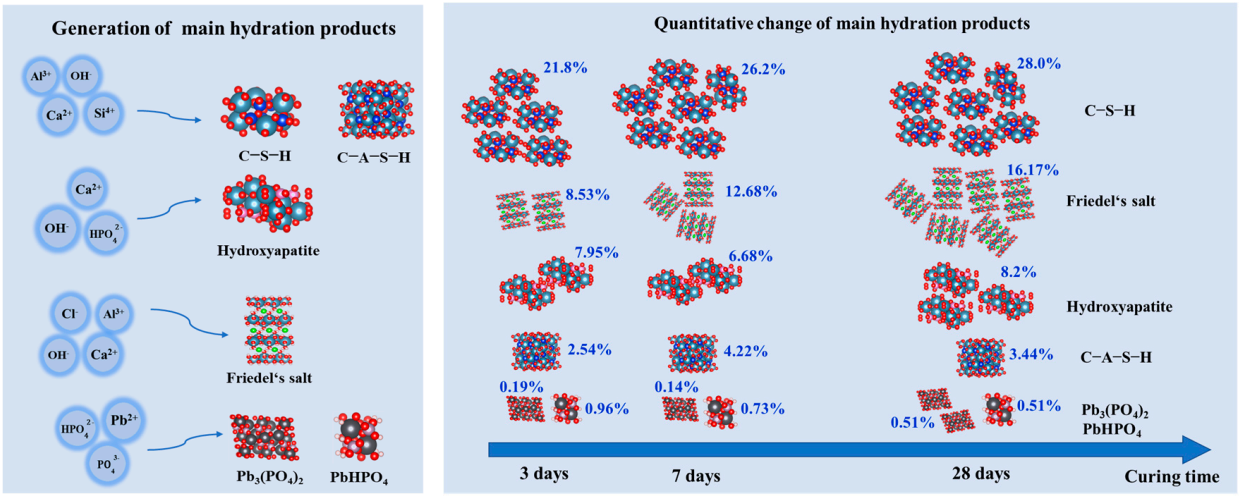

Figure 8. The quantitative change of the main hydration products of MSWCM paste with MSWI fly ash.

Table 7. Quantitative results of sample MF1 using the Rietveld method.

Minerals	Chemical Formula	Rietveld Quantitative Results Contents/Mass %		
		3 d R_{wp} = 7.81% R_{exp} = 6.07%	**7 d** R_{wp} = 7.77% R_{exp} = 6.12%	**28 d** R_{wp} = 7.70% R_{exp} = 6.12%
Portlandite	$Ca(OH)_2$	0.96 (2) [a]	0.17 (1)	0
C-S-H	$Ca_5Si_6O_{16}(OH)\cdot 4H_2O$	21.8 (1)	26.2 (1)	28.0 (1)
Periclase	MgO	0.49 (2)	2.32 (2)	1.43 (3)
Halite	NaCl	11.22 (3)	12.27 (3)	6.76 (3)
Sylvite	KCl	4.57 (2)	5.05 (2)	1.62 (2)
Mayenite	$Ca_{12}Al_{14}O_{33}$	0.86 (4)	0	0
Gypsum	$CaSO_4\cdot 2H_2O$	5.52 (4)	5.17 (4)	5.79 (4)
Ettringite	$3CaO\cdot Al_2O_3\cdot 3CaSO_4\cdot 32H_2O$	0	2.16 (1)	0.49 (1)
Friedel's salt	$3CaO\cdot Al_2O_3\cdot CaCl_2\cdot 10H_2O$	8.53 (5)	12.68 (5)	16.17 (6)
Grossite	$CaAl_4O_7$	1.36 (3)	2.09 (5)	1.08 (3)
Calcite	$CaCO_3$	6.57 (5)	5.22 (5)	9.84 (5)
K_3PO_4	-	8.56 (3)	6.54 (3)	8.62 (3)
PbO_2	-	0.68 (1)	0.27 (1)	0.41 (1)
$AlPO_4$	-	7.07 (1)	7.57 (1)	6.71 (1)
Hydroxyapatite	$Ca_5(PO_4)_3(OH)$	7.95 (5)	6.68 (45)	8.2 (6)
$CaCl_2$	-	0.28 (1)	0.52 (1)	0.39 (1)
$PbHPO_4$	-	0.96 (1)	0.73 (1)	0.51 (1)
$Pb_3(PO_4)_2$	-	0.19 (1)	0.14 (1)	0.51 (1)
C-A-S-H	$3CaO\cdot Al_2O_3\cdot 2SiO_2\cdot 2H_2O$	2.54 (5)	4.22 (4)	3.44 (4)
Carnallite	$KCl\cdot MgCl_2\cdot 6H_2O$	9.87 (6)	-	-
Sum		100.0	100.0	100.0

[a] Standard deviation.

4. Conclusions

This study proposed the preparation of multiple solid waste-based cementitious material (MSWCM) from blast furnace slag (BFS), steel slag (SS), desulfurization ash (DA) and phosphoric acid sludge (PAS). The Rietveld method was applied for the qualitative and quantitative analysis of the hydration products of pure MSWCM pastes and MSWCM pastes with MSWI fly ash. The immobilization mechanism of MSWI fly ash by MSWCM binders was explored in depth. The main conclusions can be drawn as follows:

(a) The optimal mass ratios of BFS:SS:DA:PAS for MSWCM preparation were 36:32:12:20 (w.t.%). The compressive strength of MSWCM with 80% MSWI fly ash content was 2.9 MPa during the 28-day curing period, which met the standard requirements. The

leachability of As, Pb, Cr and Zn were far below Toxicity Characteristic Leaching Procedure (TCLP) standard requirement and the threshold value specified in Standard GB16889-2008.

(b) The XRD analysis showed that the phase composition of the hydrated product was relatively complex. The most obvious diffraction peak in the pure MSWCM pastes was calcium carbonate and the main hydration products were hydroxyapatite, ettringite and calcium silicate hydrate (C-S-H and C-A-S-H). In contrast, strong peaks for chlorine salts such as halite and sylvite were observed in the mixed sample of 70% MSWCM and 30% MSWI fly ash. Additionally, small amounts of lead phosphate salts ($PbHPO_4$ and $Pb_3(PO_4)_2$) were formed.

(c) The refinements of the samples MF0 and MF1 got low R_{wp} and R_{exp} values, which indicated that the refinement results were acceptable and reasonable. Most of the hydration reactions had started at the initial stage of curing and reacted quickly to form a large amount of hydration products. For the pure MSWCM paste, the main hydration products were C-S-H, hydroxyapatite and ettringite. With increased curing time, the content of ettringite increased obviously. For the MSWCM paste with MSWI fly ash, the content of C-S-H and Friedel's salt increased significantly with increased curing time. During a curing period of 3 days to 28 days, the content of C-S-H and Friedel's salt increased by 22% and 90%, respectively. Phosphate ions reacted with Pb to form a small amount of $PbHPO_4$ and $Pb_3(PO_4)_2$. It was further confirmed that phosphate had a good curing effect on lead ions. The hydration process could be deduced and evidenced by the changes in the content of the hydration products.

Author Contributions: Conceptualization, X.W. and P.F.; methodology, investigation, data curation, X.W., W.D., J.S. and M.X.; writing—original draft preparation, X.W.; writing—review and editing, X.W. and P.F.; supervision, project administration, P.F.; funding acquisition, X.W. and P.F. All authors have read and agreed to the published version of the manuscript.

Funding: This research was funded by the Open Foundation of State Key Laboratory of Mineral Processing (grant numbers BGRIMM-KJSKL-2022-22), the Key Research and Development Program of Hebei Province (grant numbers 22373809D) and the National Key Research and Development Program of China (grant numbers 2018YFC1900604).

Data Availability Statement: The data presented in this study are available on request from the corresponding author.

Conflicts of Interest: The authors declare no conflict of interest.

References

1. Song, J.; Sun, Y.; Jin, L. PESTEL analysis of the development of the waste-to-energy incineration industry in China. *Renew. Sustain. Energ. Rev.* **2017**, *80*, 276–289. [CrossRef]
2. Liu, A.; Ren, F.; Lin, W.L.Y.; Wang, J.Y. A review of municipal solid waste environmental standards with a focus on incinerator residues. *Int. J. Sustain. Built Environ.* **2015**, *4*, 165–188. [CrossRef]
3. Moon, M.H.; Kang, D.; Lim, H.; Oh, J.E.; Chang, Y.S. Continuous fractionation of fly ash particles by SPLITT for the investigation of PCDD/Fs levels in different sizes of insoluble particles. *Environ. Sci. Technol.* **2002**, *36*, 4416–4423. [CrossRef] [PubMed]
4. Guo, Y.; Glad, T.; Zhong, Z.Z.; He, R.N.; Tian, J.P.; Chen, L.J. Environmental life-cycle assessment of municipal solid waste incineration stocks in Chinese industrial parks. *Resour. Conserv. Recycl.* **2018**, *139*, 387–395. [CrossRef]
5. Cucchiella, F.; D'Adamo, I.; Gastaldi, M. Sustainable waste management: Waste to energy plant as an alternative to landfill. *Energy Convers. Manag.* **2017**, *131*, 18–31. [CrossRef]
6. Zhu, Y.; Ye, Z.; Ren, L.; Zhong, Y.; Zhou, W. Experimental Study on Municipal Solid Waste Incineration Fly Ash in Conjunction with Construction Waste to Burn Ceramics. *Environ. Eng.* **2023**, 1–11. Available online: http://kns.cnki.net/kcms/detail/11.2097.X.20230411.1337.010.html (accessed on 20 June 2023).
7. Zhang, Y.; Wang, L.; Chen, L.; Ma, B.; Zhang, Y.; Ni, W.; Tsang, D.C.W. Treatment of municipal solid waste incineration fly ash: State-of-the-art technologies and future perspectives. *J. Hazard. Mater.* **2021**, *411*, 125–132. [CrossRef]
8. Nikravan, M.; Ramezanianpour, A.; Maknoon, R. Study on physiochemical properties and leaching behavior of residual ash fractions from a municipal solid waste incinerator (MSWI) plant. *J. Environ. Manag.* **2020**, *260*, 110042. [CrossRef]
9. Loginova, E.; Proskurnin, M.; Brouwers, H.J.H. Municipal solid waste incineration (MSWI) fly ash composition analysis: A case study of combined chelatant-based washing treatment efficiency. *J. Environ. Manag.* **2019**, *235*, 480–488. [CrossRef]

10. Lombardi, F.; Mangialardi, T.; Piga, L. Mechanical and leaching properties of cement solidified hospital solid waste incinerator fly ash. *Waste Manag.* **1998**, *18*, 99–106. [CrossRef]
11. Luo, H.W.; Cheng, Y.; He, D.; Yang, E. Review of leaching behavior of municipal solid waste incineration (MSWI) ash. *Sci. Total Environ.* **2019**, *668*, 90–103. [CrossRef]
12. Bie, R.S.; Chen, P.; Song, X.F.; Ji, X.Y. Characteristics of municipal solid waste incineration fly ash with cement solidificationtreatment. *J. Energy Inst.* **2016**, *89*, 704–712. [CrossRef]
13. Quina, M.J.; Bordado, J.C.; Quinta-Ferreira, R.M. Treatment and use of air pollution control residues from MSW incineration: An overview. *Waste Manag.* **2008**, *28*, 2097–2121. [CrossRef]
14. Du, B.; Li, J.; Wen, F.; Liu, J. Comparison of long-term stability under natural ageing between cement solidified and chelator-stabilised MSWI fly ash. *Environ. Pollut.* **2019**, *250*, 68–78. [CrossRef]
15. Ma, W.; Chen, D.; Pan, M.; Gu, T.; Zhong, L.; Chen, G.; Yan, B.; Cheng, Z. Performance of chemical chelating agent stabilization and cement solidification on heavy metals in mswi fly ash: A comparative study. *J. Environ. Manag.* **2019**, *247*, 169–177. [CrossRef]
16. Leist, M.; Casey, R.J.; Caridi, D. The management of arsenic wastes: Problems and prospects. *J. Hazard. Mater.* **2000**, *76*, 125–138. [CrossRef]
17. Chen, L.; Wang, L.; Zhang, Y.; Ruan, S.; Mechtcherine, V.; Tsang, D.C.W. Roles of biochar in cement-based stabilization/solidification of municipal solid waste incineration fly ash. *Chem. Eng. J.* **2022**, *430*, 132972. [CrossRef]
18. Gineys, N.; Aouad, G.; Damidot, D. Managing trace elements in Portland cement—Part I: Interactions between cement paste and heavy metals added during mixing as soluble salts. *Cem. Concr. Compos.* **2010**, *32*, 563–570. [CrossRef]
19. Tang, P. Stabilization/solidification of municipal solid waste incineration bottom ash. In *Low Carbon Stabilization and Solidification of Hazardous Wastes*; Tsang, D.C.W., Wang, L., Eds.; Elsevier: Amsterdam, The Netherlands, 2022; pp. 157–174.
20. Wang, L.; Chen, L.; Cho, D.W.; Tsang, D.C.W.; Yang, J.; Hou, D.; Baek, K.; Kua, H.W.; Poon, C.S. Novel synergy of Si-rich minerals and reactive MgO for stabilization/solidification of contaminated sediment. *J. Hazard. Mater.* **2019**, *365*, 695–706. [CrossRef]
21. Wang, L.; Yu, K.; Li, J.S.; Tsang, D.C.W.; Poon, C.S.; Yoo, J.C.; Baek, K.; Ding, S.; Hou, D.; Dai, J.G. Low-carbon and low-alkalinity stabilization/solidification of high-Pb contaminated soil. *Chem. Eng. J.* **2018**, *351*, 418–427. [CrossRef]
22. Dutre, V.; Vandecasteele, C. Immobilization mechanism of arsenic in waste solidified by using cement and lime. *Environ. Sci. Technol.* **1998**, *32*, 2782–2787. [CrossRef]
23. Arthur, S.; Saitoh, M.; Pal, S.K. *Advances in Civil Engineering: Select Proceedings of ICACE 2020*; Springer Nature: Berlin/Heidelberg, Germany, 2021; Volume 184, pp. 55–63.
24. Abdollahi, S.; Zarei, Z. Reduction of CO_2 emission and production costs by using pozzolans in Lamerd cement factory. *Iran. J. Chem. Chem. Eng.* **2018**, *37*, 223–230.
25. Ferreira, C.; Ribeiro, A.; Ottosen, L. Possible applications for municipal solid waste fly ash. *J. Hazard. Mater.* **2003**, *96*, 201–216. [CrossRef] [PubMed]
26. Zhang, Y.Y.; Zhang, S.Q.; Ni, W.; Yan, Q.H.; Gao, W.; Li, Y.Y. Immobilisation of high-arsenic-containing tailings by using metallurgical slag-cementing materials. *Chemosphere* **2019**, *223*, 117–123. [CrossRef] [PubMed]
27. Deng, W.; Fu, P.; Fang, G.; Zhu, W.; Li, S.; Wang, X.; Xue, T.; Chen, Y. Solidification/Stabilization of MSWI Fly Ash Using a Novel Metallurgical Slag-Based Cementitious Material. *Minerals* **2022**, *12*, 599. [CrossRef]
28. Lampris, C.; Stegemann, J.A.; Cheeseman, C.R. Chloride leaching from air pollution control residues solidified using ground granulated blast furnace slag. *Chemosphere* **2008**, *73*, 1544–1549. [CrossRef]
29. Xia, Z.R.; Lin, J.; Chi, Y.W.; Wang, J.D. Hydrothermal solidification mechanism of calcareous materials and resource utilization of desulfurization ash. *Glass Phys. Chem.* **2020**, *46*, 53–63.
30. Wang, C.Q.; Tan, K.F.; Xu, X.X.; Wang, P.X. Effect of activators, admixtures and temperature on the early hydration performance of desulfurization ash. *Constr. Build. Mater.* **2014**, *70*, 322–331. [CrossRef]
31. Jang, G.G.; Ladshaw, A.; Keum, J.K.; Zhang, P.; Tsouris, C. Continuous-flow centrifugal solid/liquid separation for the recovery of rare-earth elements containing particles from phosphoric acid sludge. *Ind. Eng. Chem. Res.* **2020**, *59*, 21901–21913. [CrossRef]
32. Sugiyama, S.; Imanishi, K.; Shimoda, N.; Liu, J.C.; Satou, H.; Yamamoto, T. Recovery of phosphoric acid and calcium phosphate from dephosphorization slag. *J. Chem. Eng. Jpn.* **2021**, *54*, 467–471. [CrossRef]
33. Fan, C.; Wang, B.; Zhang, T. Review on Cement Stabilization/Solidification of Municipal Solid Waste Incineration Fly Ash. *Adv. Mater. Sci. Eng.* **2018**, *2018*, 5120649. [CrossRef]
34. Su, Y.; Yang, J.; Liu, D.; Zhen, S.; Lin, N.; Zhou, Y. Effects of municipal solid waste incineration fly ash on solidification/stabilization of cd and pb by magnesium potassium phosphate cement. *J. Environ. Chem. Eng.* **2016**, *4*, 259–265. [CrossRef]
35. Buj, I.; Torras, J.; Rovira, M.; Pablo, J.D. Leaching behaviour of magnesium phosphate cements containing high quantities of heavy metals. *J. Hazard. Mater.* **2010**, *175*, 789–794. [CrossRef]
36. Mahieux, P.Y.; Aubert, J.E.; Cyr, M.; Coutand, M.; Husson, B. Quantitative mineralogical composition of complex mineral wastes-contribution of the Rietveld method. *Waste Manag.* **2010**, *30*, 378–388. [CrossRef]
37. Rietveld, H.M. A profile refinement method for nuclear and magnetic structures. *J. Appl. Crystallogr.* **1969**, *2*, 65–71. [CrossRef]
38. Xia, S.; Lin, R.; Cui, X.; Shan, J. The application of orthogonal test method in the parameters optimization of PEMFC under steady working condition. *Int. J. Hydrogen Energy* **2016**, *41*, 11380–11390. [CrossRef]
39. Taguchi, G.; Phadke, M.S. Quality Engineering through Design Optimization. In *Quality Control, Robust Design, and the Taguchi Method*; Springer: Berlin/Heidelberg, Germany, 1989; pp. 77–96.

40. Taut, T.; Kleeberg, R.; Bergmann, J. The new seifert Rieveld program BGMN and its application to quantitative phase analysis. *Mater. Struct.* **1998**, *5*, 57–66.
41. Bergmann, J.; Friedel, P.; Kleeberg, R. BGMN-a new fundamental parameters based Rietveld program for laboratory X-ray sources; it's use in quantitative analysis and structure investigations. *CPD Newsl.* **1998**, *20*, 5–8.
42. Fan, C.; Wang, B.; Qi, Y.; Liu, Z. Characteristics and leaching behavior of MSWI fly ash in novel solidification/stabilization binders. *Waste Manag.* **2021**, *131*, 277–285. [CrossRef]
43. Ren, P.; Ling, T.C. Roles of chlorine and sulphate in MSWIFA in GGBFS binder: Hydration, mechanical properties and stabilization considerations. *Environ. Pollut.* **2021**, *284*, 117175. [CrossRef]
44. Forestier, L.; Libourel, G. Characterization of flue gas residues from municipal solid waste combustors. *Environ. Sci. Technol.* **1998**, *32*, 2250–2256. [CrossRef]
45. Chi, M.; Huang, R. Binding mechanism and properties of alkali-activated fly ash/slag mortars. *Constr. Build. Mater.* **2013**, *40*, 291–298. [CrossRef]
46. Patil, A.A.; Chore, H.S.; Dodeb, P.A. Effect of curing condition on strength of geopolymer concrete. *Adv. Concrete Constr.* **2014**, *2*, 29–37. [CrossRef]
47. Ren, J.; Zhang, Z.; Wang, M.; Guo, G.; Du, P.; Li, F. Phosphate-induced differences in stabilization efficiency for soils contaminated with lead, zinc, and cadmium. *Front. Environ. Sci. Eng.* **2018**, *12*, 10. [CrossRef]
48. Cao, X.; Wang, W.; Ma, R.; Sun, S.; Lin, J. Solidification/stabilization of Pb(2+) and Zn(2+) in the sludge incineration residue-based magnesium potassium phosphate cement: Physical and chemical mechanisms and competition between coexisting ions. *Environ. Pollut.* **2019**, *253*, 171–180. [CrossRef]